Bulletin of the Earthquake
Research Institute
Vol. 44 (1966), pp. 1465-1499

71. *Long Waves around a Convex or Concave Bottom.*

By Takao Momoi,

Earthquake Research Institute.

(Read Sept. 27, 1966.—Received Sept. 30, 1966.)

Abstract

Numerical calculations of the long waves around a convex or concave bottom have been made to elucidate the behaviors of the waves around an obstacle and to determine an effective mesh length in the construction of a refraction diagram of tsunamis.

Since the invading waves are treated as periodic ones in this work, a straightforward application of the theory to the evaluation of the effective mesh length for the leading part of tsunamis might be a little dubious (for the later phase, the present results are applicable). But when a dimension of the irregular part of the bottom (a simple hump) is small as compared with a wave-length of the incident waves, an interference effect produced by a coupling of the progressive and retrogressive waves is likely to be also small, so that the application* of the results of the periodic waves might be still possible to the leading part of tsunamis dismissing the tip of the leading waves in which no interference effect taking place in the case of periodic waves is expected. In the present study, two typical tsunamis, i.e. the Chile Tsunami and Niigata Tsunami, have been employed to determine the actual negligible dimensions of the bottom irregularities.

Furthermore, in the last section, some mention is made of the waves scattered by the submarine obstacle.

1. Introduction

The primary purpose of the present work is to determine a suitable mesh size for the construction of a refraction diagram of tsunamis with the aid of an electronic computer. The problem is treated as being three-dimensional, that is, circular mounts and basins are located in the sea of uniform depth. These forms of the bottom are possible representations of the actual sea-bed except an elongated submarine ridge.

*) Since our model is of a circular form, the application is of course limited to the evaluation of a negligible dimension of bottom irregularities of *a circular form.*

The development of the present theory has been performed in the realm of long waves, that is to say, the used equation is a simple long wave equation. For an analysis of waves of medium wave-length, it is almost certain that the selection of a basic equation is of great importance, the use of an equation in terms of velocity potential instead of a long wave equation being preferable. Such problems are reserved for a future paper.

At any rate, little seems to have been written on waves around three-dimensional submarine obstacles. Hence, we take up these problems in this article.

2. Case of Circular Table

In this section, the case of the bottom of a circular table is considered, the geometry of which is shown in Fig. 2-1. Incident waves

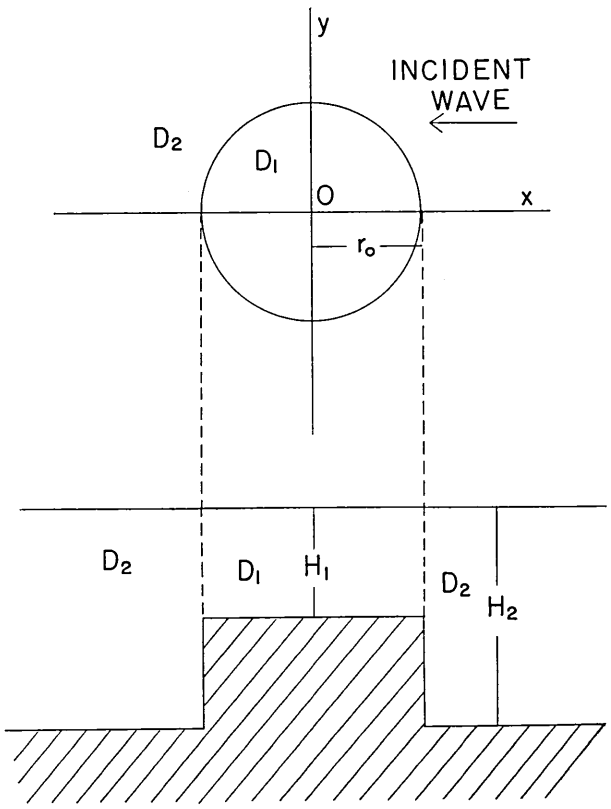

Fig. 2-1. Geometry of a used model.

are assumed to be periodic ones. This form of incident wave is also used in the subsequent sections.

(2,1) *Theory*

Referring to Fig. 2-1, the origin of the coordinates is centered at the midpoint of a circular desk.

Let (x, y) be the Cartesian coordinates and (r, θ) the polar coordinates. Then using the notations such that

ζ: wave height, H: sea depth,
t: time variable, g: gravity constant,
c: long wave velocity $(=\sqrt{gH})$,

a governing equation is given by

$$\frac{\partial^2\zeta}{\partial x^2}+\frac{\partial^2\zeta}{\partial y^2}=\frac{1}{c^2}\cdot\frac{\partial^2\zeta}{\partial t^2} \tag{2,1}$$

or

$$\frac{\partial^2\zeta}{\partial r^2}+\frac{1}{r}\cdot\frac{\partial\zeta}{\partial r}+\frac{1}{r^2}\cdot\frac{\partial^2\zeta}{\partial\theta^2}=\frac{1}{c^2}\cdot\frac{\partial^2\zeta}{\partial t^2}\ . \tag{2,2}$$

Since we are treating of a periodic problem, the above equations (2,1) and (2,2) become

$$\frac{\partial^2\zeta'}{\partial x^2}+\frac{\partial^2\zeta'}{\partial y^2}+k^2\zeta'=0 \tag{2,3}$$

or

$$\frac{\partial^2\zeta'}{\partial r^2}+\frac{1}{r}\cdot\frac{\partial\zeta'}{\partial r}+\frac{1}{r^2}\cdot\frac{\partial^2\zeta'}{\partial\theta^2}+k^2\zeta'=0 \tag{2,4}$$

where $\zeta=\zeta'\cdot\exp(+i\omega t)$

and $k=\omega/c$ (ω: angular frequency of incident waves). (2,5)

In the following, the prime of ζ' is omitted for simplicity, unless otherwise stated. This convention is followed in the subsequent sections.

Suppose that the incident waves are expressed by

$$\zeta_{in}=\zeta_0 e^{+ikx}$$

or, in complete form,

$$\zeta_{in}=\zeta_0 e^{+i\omega t+ikx}, \tag{2,6}$$

where ζ_0 is the amplitude of the incident waves, the only real part having a physical meaning, the formal solutions in domains D_1 and D_2 (for the region of the domains Fig. 2-1 should be referred to) are obtained in forms of series as follows:—

in the domain D_1,

$$\zeta_1 = \sum_{m=0}^{\infty} A_m^{(1)} \cos m\theta \cdot J_m(k_1 r) \; ; \tag{2,7}$$

in the domain D_2,

$$\zeta_2 = \zeta_0 e^{+ikx} + \sum_{m=0}^{\infty} A_m^{(2)} \cos m\theta \cdot H_m^{(2)}(k_2 r) \; ; \tag{2,8}$$

where ζ_j $(j=1, 2)$ are the wave heights in the domains D_j $(j=1, 2)$, $A_m^{(j)}$ $(j=1, 2;\ m=0, 1, 2, \cdots)$ the unknowns to be determined by the conditions between the domains D_1 and D_2, and k_j $(j=1, 2)$ the wave numbers of the waves in the domains D_j $(j=1, 2)$ (hence $k = k_2$) which are related with long wave velocities c_j $(j=1, 2)$ in the domains D_j $(j=1, 2)$ through the relations

$$k_j = \omega / c_j \; . \tag{2,9}$$

In the expression (2,7), the finiteness of the wave amplitude in the origin $(r=0)$ is assumed so that the Bessel function of the second kind, $Y_m(k_1 r)$, is excluded, while reflected waves are assumed, in (2,8), to be outgoing scatterred waves at an infinite point from the obstacle. In both solutions, a symmetry of the phenomenon with respect to the x-axis is employed so that sine-terms are excluded from the series.

In order to determine the unknowns $A_m^{(j)}$ $(m=0, 1, 2, \cdots;\ j=1, 2)$ of (2,7) and (2,8), we have two conditions available, i.e.,

$$\left.\begin{aligned} \zeta_1 &= \zeta_2 \\ H_1 \frac{\partial \zeta_1}{\partial r} &= H_2 \frac{\partial \zeta_2}{\partial r} \end{aligned}\right\} \text{ at } r = r_0 \, , \tag{2,10}$$

where r_0 is a radius of the convex circular desk of the sea bottom and H_j $(j=1, 2)$ the depths of the sea in the domains D_j $(j=1, 2)$ respectively (see Fig. 2-1).

Substituting (2,7) and (2,8) into the conditions (2,10) and applying the operators

$$\int_0^{2\pi} \cos n\theta d\theta \qquad (n=0, 1, 2, \cdots)$$

to them, we have the following simultaneous equations:—

$$\left.\begin{aligned} &J_0(k_1r_0)A_0^{(1)}-H_0^{(2)}(k_2r_0)A_0^{(2)}=J_0(k_2r_0)\zeta_0\,,\\ &J_0'(k_1r_0)A_0^{(1)}-\frac{k_2H_2}{k_1H_1}H_0^{(2)\prime}(k_2r_0)\,A_0^{(2)}=\frac{k_2H_2}{k_1H_1}J_0'(k_2r_0)\zeta_0\,, \end{aligned}\right\} \tag{2,11}$$

$$\left.\begin{aligned} &J_m(k_1r_0)A_m^{(1)}-H_m^{(2)}(k_2r_0)A_m^{(2)}\\ &\quad=2\zeta_0\begin{cases}(-1)^nJ_{2n}(k_2r_0) & (m=2n)\,,\\ i\cdot(-1)^{n+1}J_{2n-1}(k_2r_0) & (m=2n-1)\,,\end{cases}\\ &J_m'(k_1r_0)A_m^{(1)}-\frac{k_2H_2}{k_1H_1}H_m^{(2)\prime}(k_2r_0)A_m^{(2)}\\ &\quad=2\zeta_0\frac{k_2H_2}{k_1H_1}\begin{cases}(-1)^nJ_{2n}'(k_2r_0) & (m=2n)\,,\\ i\cdot(-1)^{n+1}J_{2n-1}'(k_2r_0) & (m=2n-1)\,,\end{cases}\\ &\qquad(n=1,\,2,\,3,\,\cdots)\,, \end{aligned}\right\} \tag{2,12}$$

where the formula[1]

$$\begin{aligned} e^{+ikx}&=e^{+ikr\cos\theta}\\ &=J_0(kr)+2\sum_{m=1}^{\infty}(-1)^mJ_{2m}(kr)\cos 2m\theta\\ &\quad+2i\sum_{m=0}^{\infty}(-1)^mJ_{2m+1}(kr)\cos(2m+1)\theta \end{aligned}$$

has been used in the above reductions.

The simultaneous equations (2,11) and (2,12) are readily solved numerically with the aid of an electronic computer. In the calculation, the subroutines for obtaining the Bessel functions and solving simultaneous equations (based on a method of sweeping) are employed. Substituting the unknowns $A_m^{(j)}$ $(j=1,\,2;\ m=0,\,1,\,2,\,\cdots)$ obtained in the above into the formal expressions (2,7) and (2,8), we can elucidate the behaviors of waves around the submarine obstacle. This procedure, of course, is carried out by use of an electronic computer.

(2,2) *Numerical Computations and Determination of Mesh Size*

In this section, numerical calculations of the theory were made following the procedure described in the previous section (2,1) and their results were discussed.

Variations of the amplitude and phase in the direction $\theta=0,\ \pi/2$ and

1) S. MORIGUCHI, et al., *Sūgaku Kōshiki III* (literally, *Mathematical Formula III*) (Yuwanami Shoten, 1961), 211.

π are presented in Figs. 2-2, 2-3, $\cdots$, 2-13 for parameters $kr_0=0.2$, 0.4, $\cdots$, 2.0 and $H_2/H_1=4/3$, 4/2, 4/1.

To begin with, the variations of the amplitude are discussed.

When the waves advance along the x-axis (the direction of incidence of waves) through the midpoint of a circular obstacle, the height of the waves, referring to Figs. 2-2, 2-3 and 2-4, increases in general to take a maximum at a certain point which moves to the direction of propagation of waves as kr_0 increases and also the amount of a maximum wave height is augmented as kr_0 increases. Through Figs. 2-2, 2-3 and 2-4,

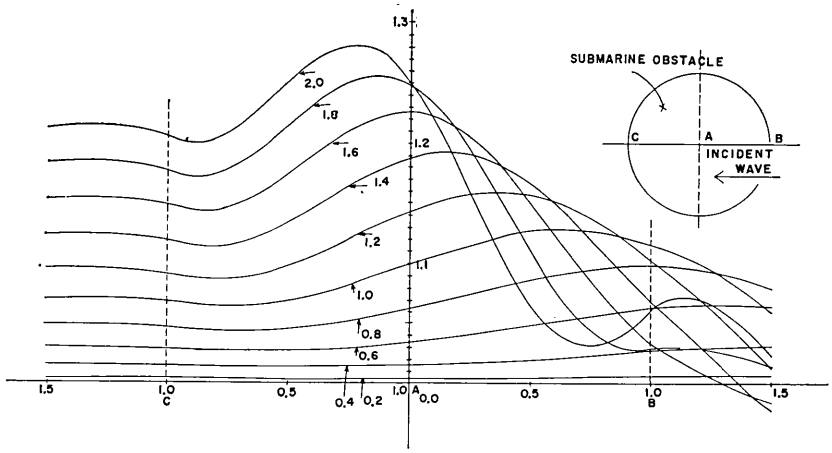

Fig. 2-2. Variation of amplitude along x-axis for a specified ratio of depth $H_2/H_1=4/3$ (the numbers stated in the curves denote the values of kr_0).

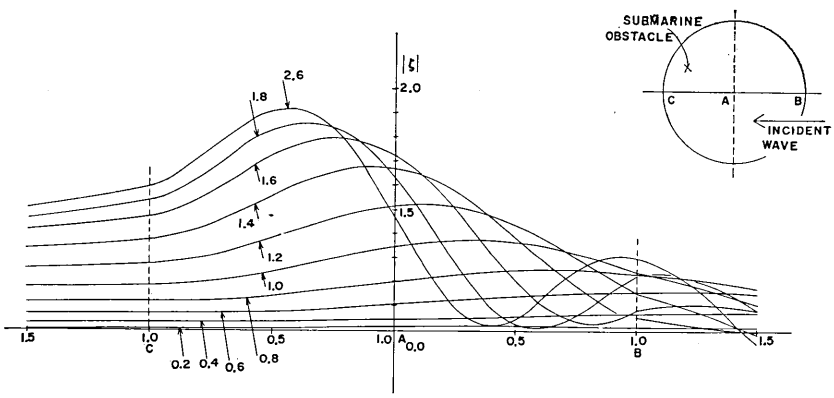

Fig. 2-3. Variation of amplitude along the x-axis for the ratio of depth $H_2/H_1=4/2$ (the numbers stated in the curves denote the values of kr_0).

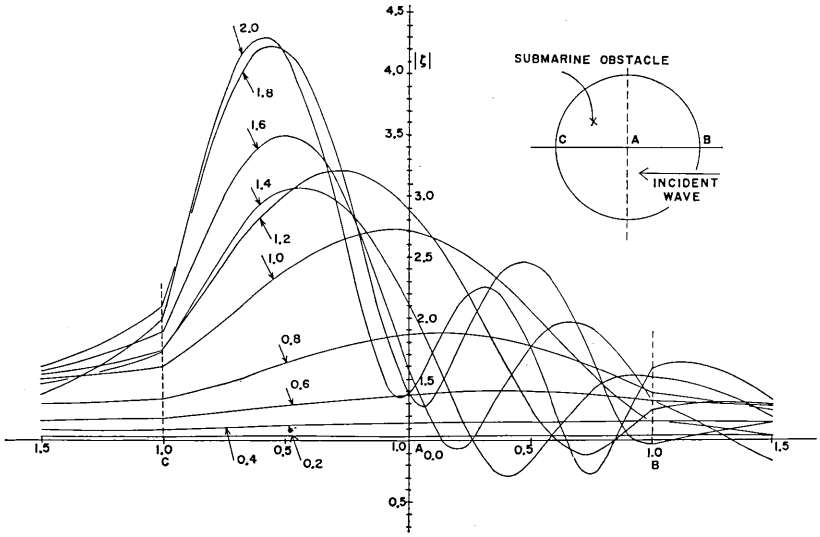

Fig. 2-4. Variation of amplitude along the x-axis for a specified ratio of depth $H_2/H_1=4/1$ (the stated numbers in the curves denote the values of kr_0).

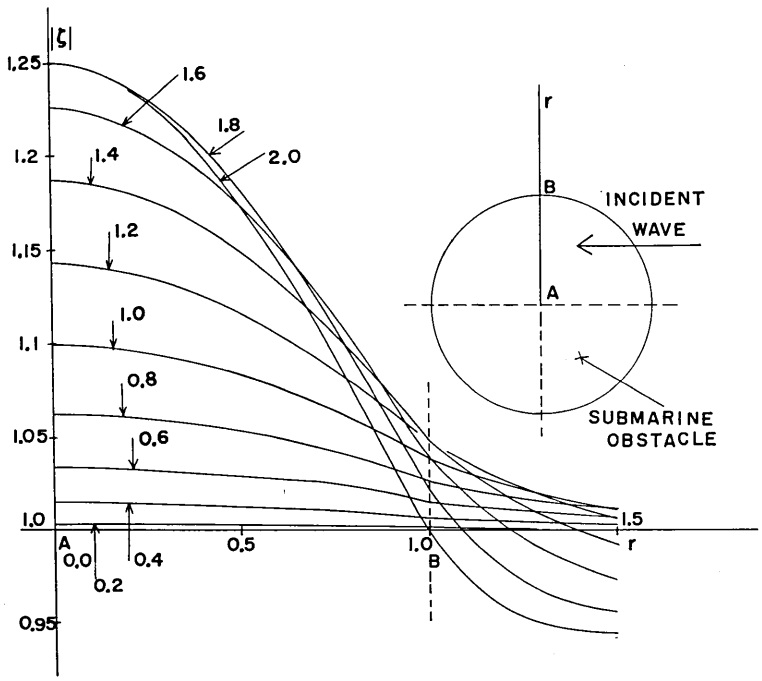

Fig. 2-5. Variation of amplitude along the y-axis for a specified ratio of depth $H_2/H_1=4/3$ (the numbers stated in the curves denote the values of kr_0).

when kr_0 is large, a valley of the amplitude (a low amplitude point) appears before the waves reaching the midpoint of the obstacle. Such an appearance of a low amplitude point is interpreted to be caused by an interference of the progressing waves and the retrograding ones which are generated at the outer margin of the obstacle.

Along the y-axis (the direction perpendicular to that of the incident waves), the variation of the amplitude is as follows. In Figs. 2–5 and 2–6, the wave heights take a maximum in the central part of the obstacle and diminish gradually leaving from the midpoint. Near the outer margin of the obstacle, those values approach a unit and some of these take a value less than a unit crossing the line $|\zeta|=1.0$. This phenomenon is considered to be resulted in by an interference of the incident and scattered waves. In Fig. 2–7 (the case for $H_2/H_1=4.0$), a slightly different situation takes places. In this case, when kr_0 becomes large ($kr_0=1.8$ and 2.0), a maximum point of the wave height appears near the margin of the obstacle and the wave height in the central part somewhat decreases. Such behavious are caused as a result of an interference of

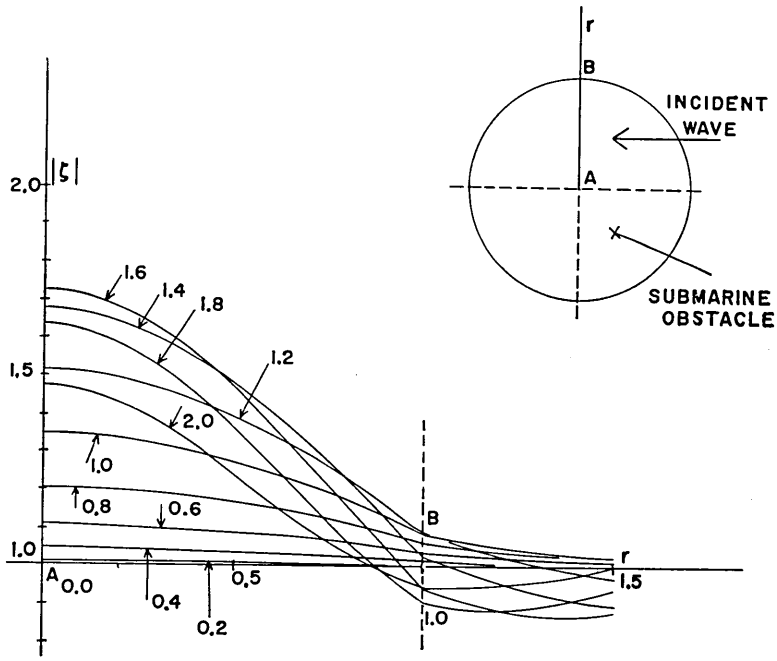

Fig. 2-6. Variation of amplitude along the y-axis for a specified ratio of depth $H_2/H_1=4/2$ (the stated numbers denote the curves relevant to a parameter kr_0).

waves which becomes notable when H_2/H_1 is large or when kr_0 increases.

Since we are now developing a theory on the basis of a long wave equation in which a vertical acceleration is not allowed for, the applicability of the present theory might be a little dubious to a problem possessing a large ratio of depth such that $H_2/H_1 \sim 4.0$. A particular emphasis therefore is not laid upon the phenomena of the waves for a ratio of depth $H_2/H_1 = 4.0$. In a future paper, the applicability of a long wave equation to a three-dimensional problem with an irregular bottom will be examined.

At any rate, passing through Figs. 2-2, 2-3, ···, 2-7, when the ratio of depth (H_2/H_1) is small or when the wave-length is large as compared with the dimension of a submarine obstacle, the effect of the obstacle

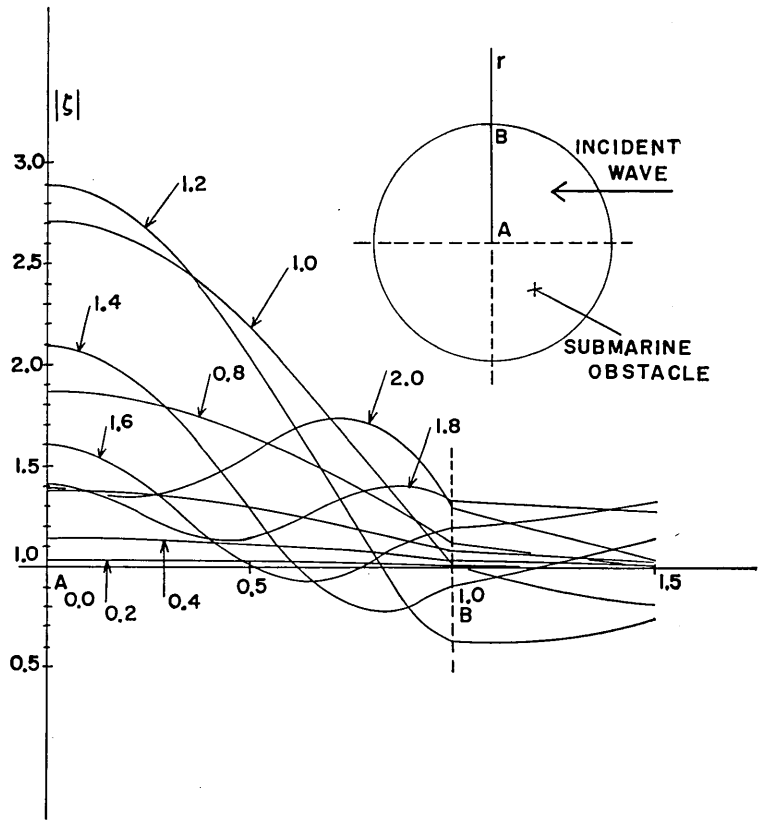

Fig. 2-7. Variation of amplitude along the y-axis for a specified ratio of depth $H_2/H_1 = 4/1$ (the stated numbers denote the curves relevant to a parameter kr_0).

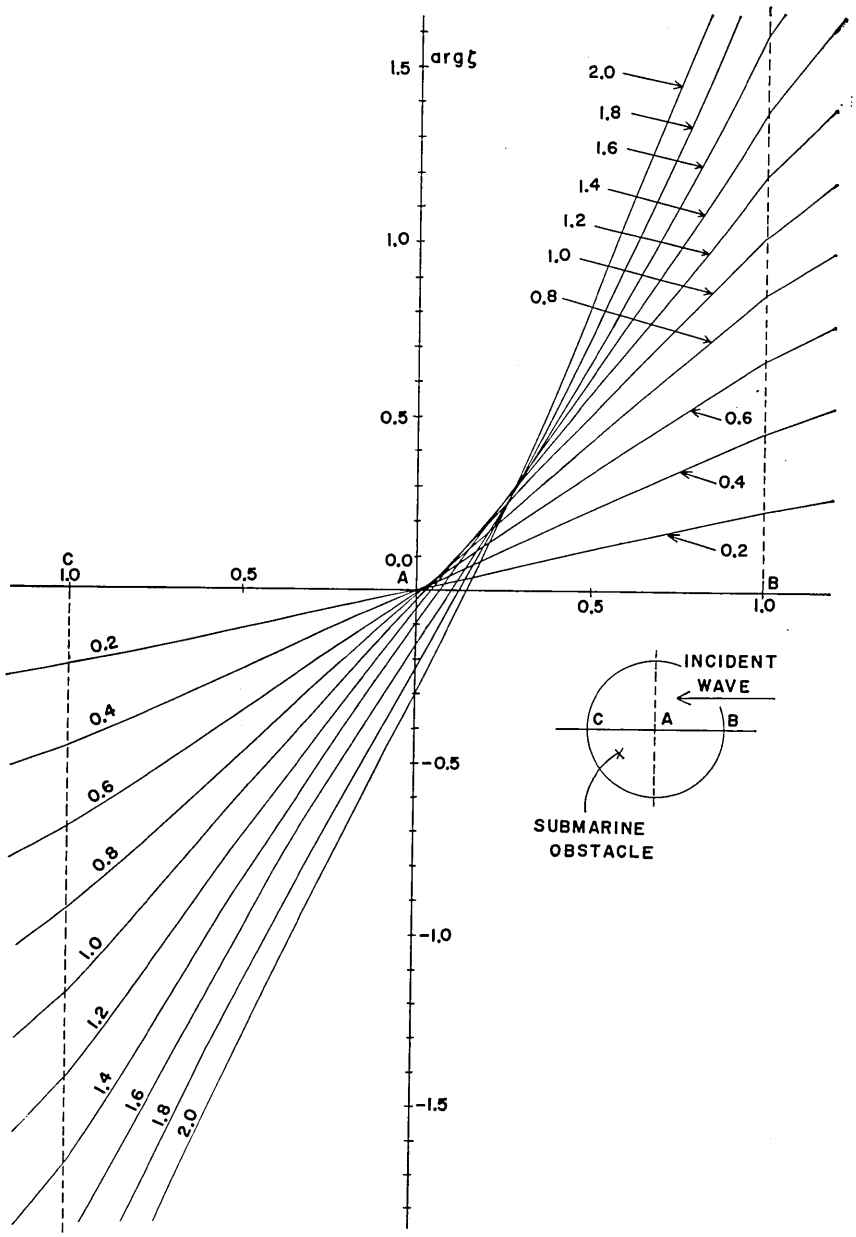

Fig. 2-8. Variation of phase along the x-axis for the ratio of depth $H_2/H_1=4/3$ (the stated numbers in the curves denote the values of kr_0).

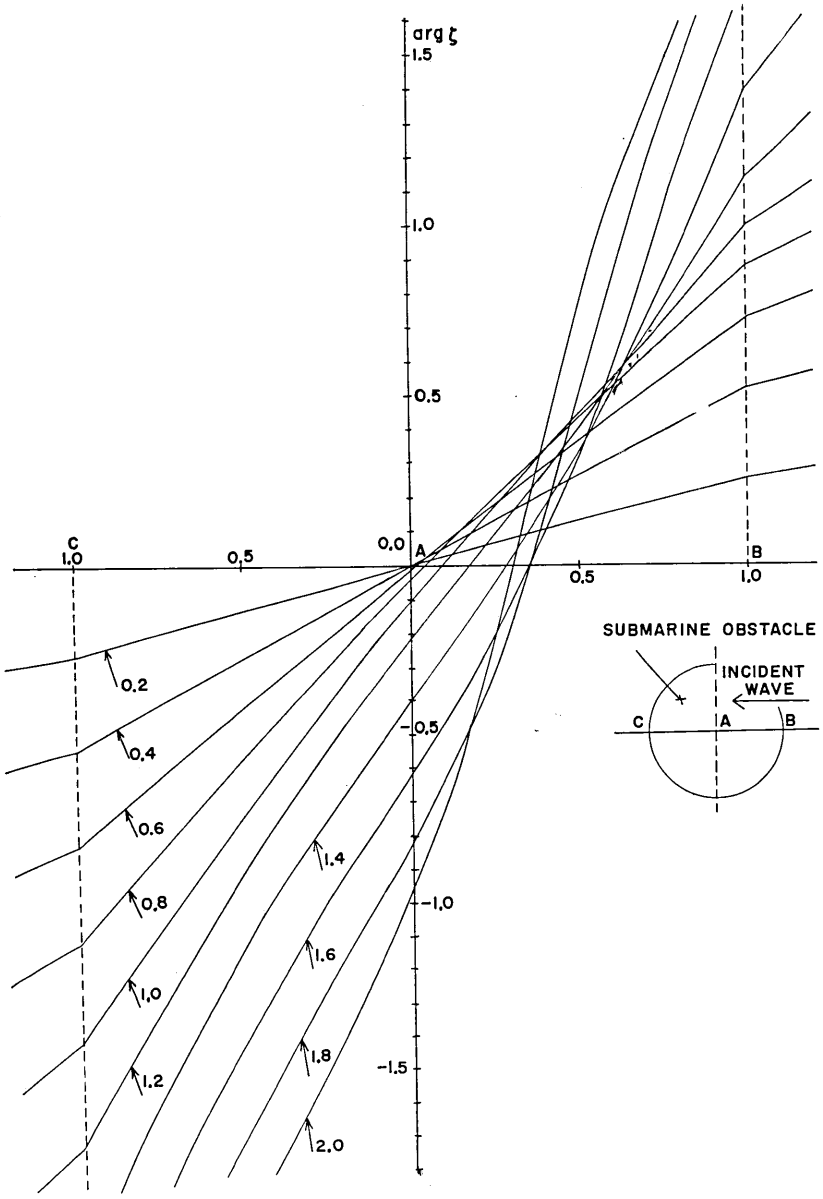

Fig. 2-9. Variation of phase along the x-axis for a specified ratio of depth $H_2/H_1=4/2$ (the stated numbers in the curves denote the values of kr_0).

upon the amplitude of the invading waves is found to be small.

Let us next consider the variation of phase. Through Figs. 2-8, 2-9 and 2-10 (the variations of phase along the x-axis), it is found that a retardation of phase at the midpoint of the obstacle begins to be great as kr_0 increases for a given ratio of depth H_2/H_1 or as H_2/H_1 increases for a given kr_0. Through three figures, a rapid variation of phase curves is seen for large kr_0, which is due to a shortening of a wave-length for

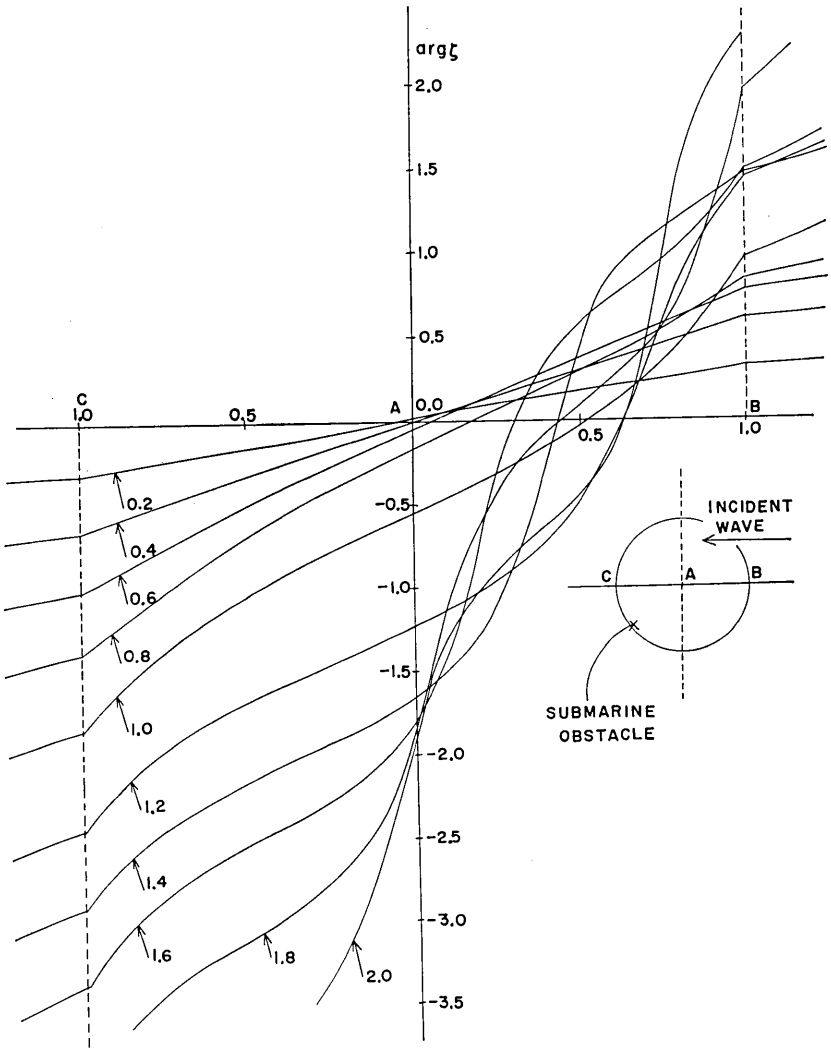

Fig. 2-10. Variation of phase along the x-axis for the ratio of depth $H_2/H_1=4/1$ (the numbers stated in the curves denote a parameter kr_0).

augmentation of kr_0. Further, a gentle transition of phase curve is seen in Figs. 2-8 and 2-9 (case for $H_2/H_1=4/3$ and 2.0) for a change of kr_0, while such gentleness disappears in Fig. 2-10 (case of $H_2/H_1=4.0$). This situation might be resulted in by a marked interference of waves advancing and retrograding over the submarine obstacle, which begins to be severe for a large ratio of depth (H_2/H_1) or large kr_0.

Noting the variations along the y-axis which are shown in Figs. 2-11, 2-12 and 2-13, it is found that the component of the waves in this axis

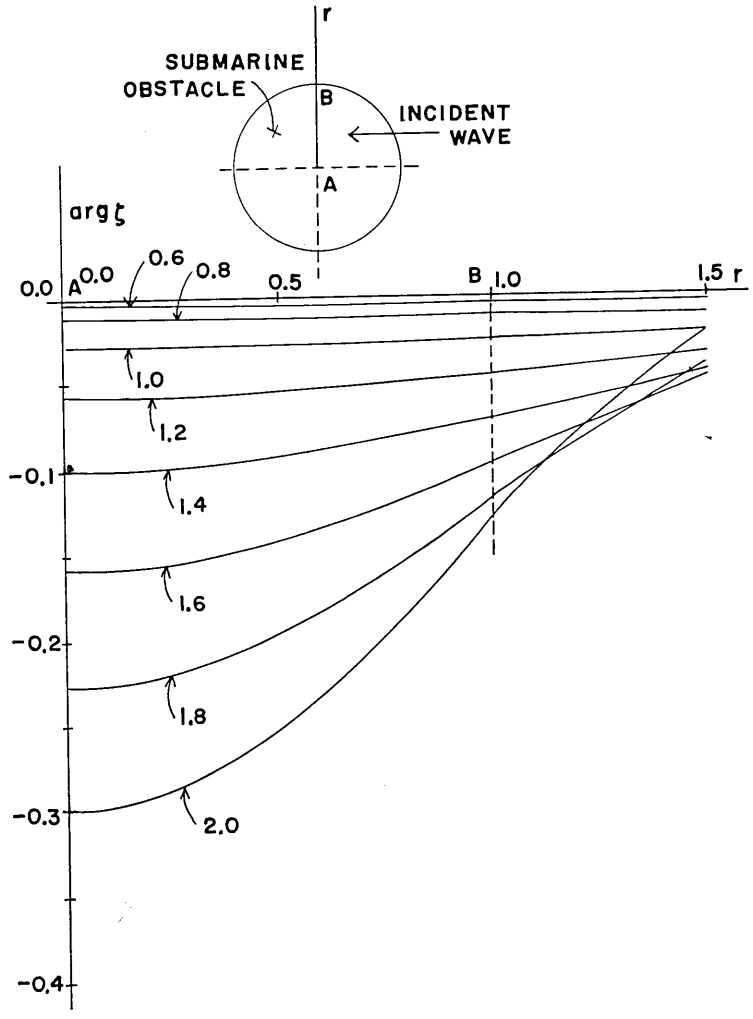

Fig. 2-11. Variation of phase along the y-axis for a specified ratio of depth $H_2/H_1=4/3$ (the numbers stated in the curves denote the values of kr_0).

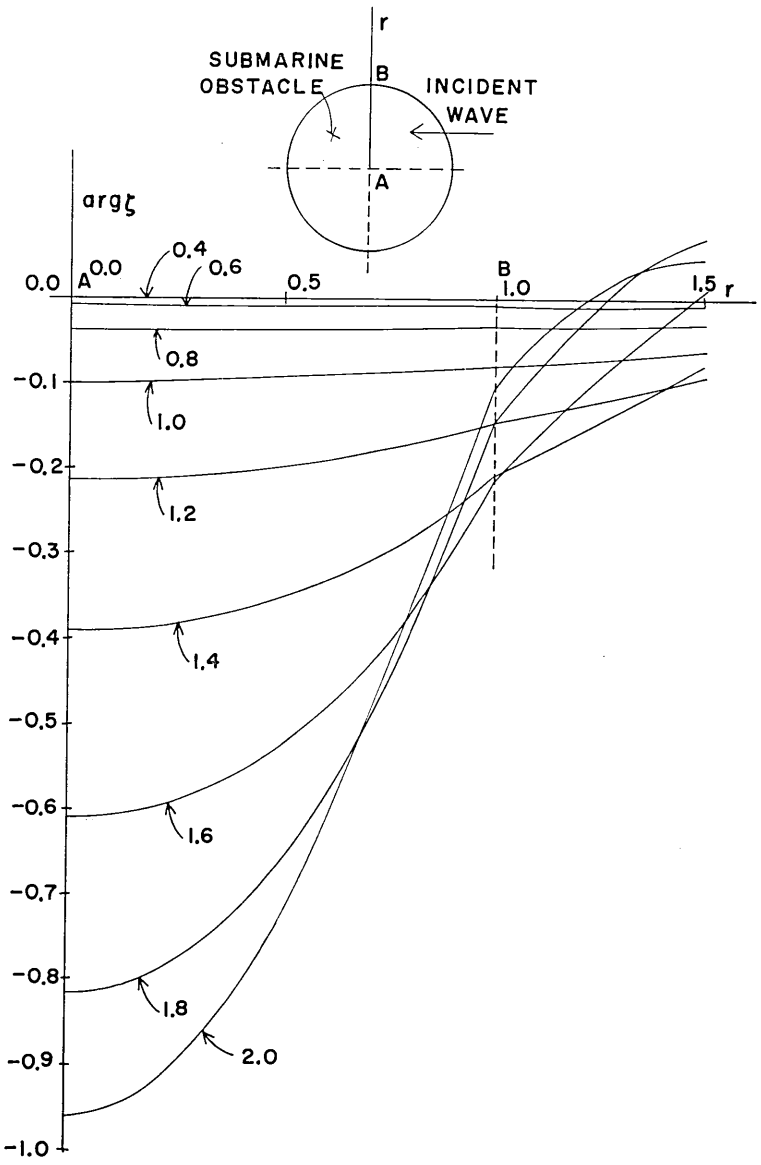

Fig. 2-12. Variation of phase along the y-axis for a specified ratio of depth $H_2/H_1=4/2$ (the numbers stated in the curves denote the values of kr_0).

is in a sense advancing towards the midpoint of the obstacle. Approaching the center, this component of the velocity begins to be small to vanish at the very point of the center of the obstacle. In the cases of $H_2/H_1=4/3$ and 2.0 (Figs. 2-11 and 2-12), the converging effect of the circular obstacle upon the waves becomes greater with an increase of kr_0 for a given ratio of depth or with an increase of H_2/H_1 for a given kr_0. In Fig. 2-13 (case of $H_2/H_1=4.0$), this feature is not seen definitely. For the range beyond 1.4, the above feature in particular disappears. This is caused as a result of an increase of interference of waves, which is

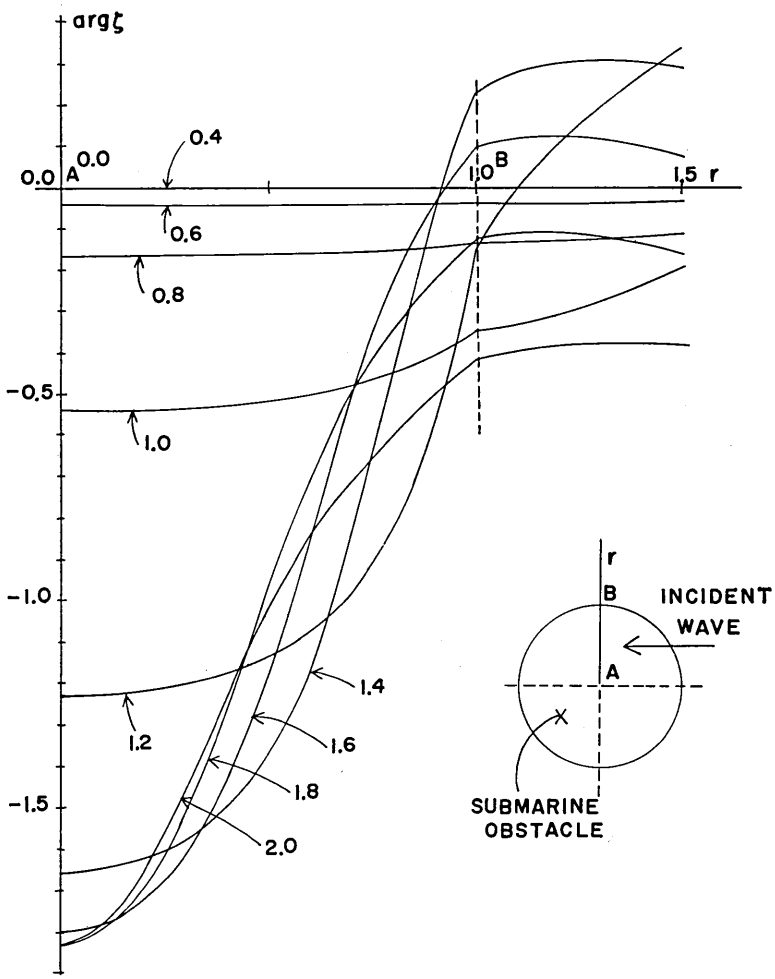

Fig. 2-13. Variation of phase along the y-axis for the ratio of depth $H_2/H_1=4/1$ (the numbers stated in the curves denote the values of kr_0).

considered as beginning to be more notable with augmentations of the ratio of depth and kr_0.

In construction of a refraction diagram of tsunamis by use of an electronic computer, the sea is covered with nets of an appropriate mesh size. At the intersecting points, the depths of the sea are represented. In drafting the above refraction diagram, a determination of a mesh size is required by a suitable means, but so far we have no definite knowledge available for such a determination, in particular for a three-dimensional case. In the present study, the theory has been developed under the assumption that the invading waves are periodic. Therefore, an estimation of the effect of the obstacle upon the leading waves of actual tsunamis by use of the result of the present calculation might be inappropriate, the application supposedly being limited to the waves of a later phase. In spite of this situation, when kr_0 is small (a resonance effect due to the obstacle is then likely to be small), the result of a periodic case is considered to be still applicable to the evaluation of a mesh size when drafting a refraction diagram for the leading part of waves*. By the above reasoning, a suitable mesh length is determined from the result of the present calculation.

If one sets up a hypothetical criterion in such a way that, when a maximum wave height is suppressed below 1.1 times that of the incident waves, the irregularity of the bottom can be neglected, the following ranges of bottom irregularities are then negligible in constructing a refraction diagram, i.e.,

$$kr_0=0\sim0.8 \quad \text{for } H_2/H_1=4/3\,,$$
$$kr_0=0\sim0.4 \quad \text{for } H_2/H_1=2.0\ (=4/2)\,,$$
and
$$kr_0=0\sim0.3 \quad \text{for } H_2/H_1=4.0\ (=4/1)\,,$$

which are obtained from Figs. 2-2, 2-3 and 2-4.

Converting the above values to the relation of $D(=2r_0)$ to λ (a wavelength), we have:—

$$\left.\begin{aligned} D/\lambda&=0\sim0.25 \quad \text{for } H_2/H_1=4/3\,,\\ D/\lambda&=0\sim0.13 \quad \text{for } H_2/H_1=4/2\,,\\ D/\lambda&=0\sim0.10 \quad \text{for } H_2/H_1=4/1\,. \end{aligned}\right\} \tag{2,13}$$

In order to estimate a negligible length of bottom irregularities on the occasion of actual tsunamis, two types of tsunamis are taken up, i.e.,

* precluding the tip of the leading waves.

the Chile Tsunami of May 24, 1960 and the Niigata Tsunami of June 16, 1964. The former represents far-field tsunamis which have a long wave-length of a period of about 40 minutes and the latter near-field tsunamis with a period of 20 minutes. Assuming the mean depth of the Pacific Ocean as 4,000 m and that of the surrounding sea of the wave origin of the Niigata Tsunami as 500 m, the above values of the period of both tsunamis are converted to wave-lengths, that is to say,

$$\left.\begin{aligned} &\lambda = 480\ \text{km} \quad \text{for the Chile Tsunami} \\ \text{and} \quad &\lambda = 80\ \text{km} \quad \text{for the Niigata Tsunami.} \end{aligned}\right\} \tag{2,14}$$

Using (2,13) and (2,14), the negligible scale D of the bottom irregularities becomes as follows.

In the case of the Chile Tsunami,

$$\left.\begin{aligned} D &= 0 \sim 120\ \text{km} \quad \text{for } H_2/H_1 = 4/3\,, \\ D &= 0 \sim 62\ \text{km} \quad \text{for } H_2/H_1 = 4/2\,, \\ D &= 0 \sim 48\ \text{km} \quad \text{for } H_2/H_1 = 4/1\,, \end{aligned}\right\} \tag{2,15}$$

and in the case of the Niigata Tsunami,

$$\left.\begin{aligned} D &= 0 \sim 20\ \text{km} \quad \text{for } H_2/H_1 = 4/3\,, \\ D &= 0 \sim 10\ \text{km} \quad \text{for } H_2/H_1 = 4/2\,, \\ D &= 0 \sim 8\ \text{km} \quad \text{for } H_2/H_1 = 4/1\,, \end{aligned}\right\} \tag{2,16}$$

The above scales have been determined under the criterion that a maximum wave height over the submarine obstacle (of a convex form) does not exceed 1.1 times that of the incident waves.

If one sets up another criterion so as to suppress the maximum wave height to be negligible below 1.05 times the amplitude of the incident waves, the negligible bottom irregularities, referring to Figs. 2-2, 2-3 and 2-4, fall in the range

$$\begin{aligned} kr_0 &= 0 \sim 0.5 \quad \text{for } H_2/H_1 = 4/3\,, \\ kr_0 &= 0 \sim 0.3 \quad \text{for } H_2/H_1 = 2.0\ (=4/2)\,, \\ kr_0 &= 0 \sim 0.2 \quad \text{for } H_2/H_1 = 4.0\ (=4/1)\,, \end{aligned}$$

These values are converted to the ratios D to λ as follows.

$$\left.\begin{aligned} D/\lambda &= 0 \sim 0.16 \quad \text{for } H_2/H_1 = 4/3\,, \\ D/\lambda &= 0 \sim 0.10 \quad \text{for } H_2/H_1 = 4/2\,, \\ D/\lambda &= 0 \sim 0.06 \quad \text{for } H_2/H_1 = 4/1\,, \end{aligned}\right\} \tag{2,17}$$

In applying the above relations (2,17) to the cases of the Chile and Niigata Tsunamis, the scales D to be neglected are, by use of (2,14):—

in the case of the Chile Tsunami,

$$\left.\begin{aligned} D&=0\sim 77\ \text{km} \quad \text{for } H_2/H_1=4/3\,,\\ D&=0\sim 48\ \text{km} \quad \text{for } H_2/H_1=4/2\,,\\ D&=0\sim 29\ \text{km} \quad \text{for } H_2/H_1=4/1\,, \end{aligned}\right\} \tag{2,18}$$

and in the case of the Niigata Tsunami,

$$\left.\begin{aligned} D&=0\sim 13\ \text{km} \quad \text{for } H_2/H_1=4/3\,,\\ D&=0\sim\ 8\ \text{km} \quad \text{for } H_2/H_1=4/2\,,\\ D&=0\sim\ 5\ \text{km} \quad \text{for } H_2/H_1=4/1\,, \end{aligned}\right\} \tag{2,19}$$

In the foregoing estimations, we took a maximum wave height near the submarine obstacle as a criterion for determining the negligible mesh size and, referring to Figs. 2-2, 2-3 and 2-4, the transmitted waves diminish generally in wave height leaving the obstacle. Therefore, if our attention is focussed upon the waves *passing through* the obstacle (that is mostly the case, in the drafting of a refraction diagram), the negligible mesh lengths already determined might be effective enough for the passing waves to hold a desired accuracy.

If one sets up another criterion for a period of waves, one can readily obtain a negligible dimension of the bottom irregularities following the afore-mentioned procedures.

3. Case of Circular Basin

In this section, a case where the bottom has a circular basin is treated, the geometry of which is shown in Fig. 3-1.

(3,1) *Theory*

In a manner similar to the case of a circular table, the origin of the coordinates is located at the midpoint of a circular basin.

Using the same definitions and notations as those in the case of a circular table, we can arrive at exactly the same simultaneous equations that are described in (2,11) and (2,12).

The only difference is that the geometry of the present case has a concave irregularity at the bottom other than a convex one as in the previous case. That is to say,

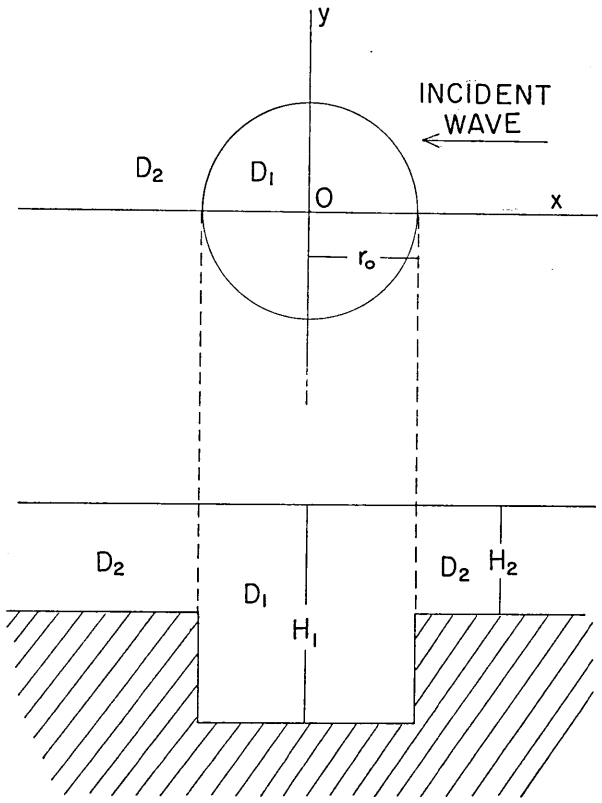

Fig. 3-1. Geometry of a used model.

$H_2 > H_1$ for the previous case (see Fig. 2-1)

and $H_2 < H_1$ for the present case (see Fig. 3-1).

At any rate, a circular portion of a convex or concave bottom with uniform depth is located in the midst of the supposed ocean of uniform depth in either case treated in Section 2 and the present Section 3. Such a uniformity of the irregular portion of the bottom is based on the simplicity of a mathematical treatment of the problem and due to the convenience of measuring a dimension of the irregular part.

Now solving the equations (2,11) and (2,12) for specified values of kr_0 $(=k_2 r_0)$ and H_2/H_1, the unknown factors $A_m^{(j)}$ $(j=1, 2;\ m=0, 1, 2, \cdots)$ in the formal expressions (2,7) and (2,8) are obtained, so that the variations of the amplitude and phase in the nearby part of the submarine obstacle begin to be known through (2,7) and (2,8).

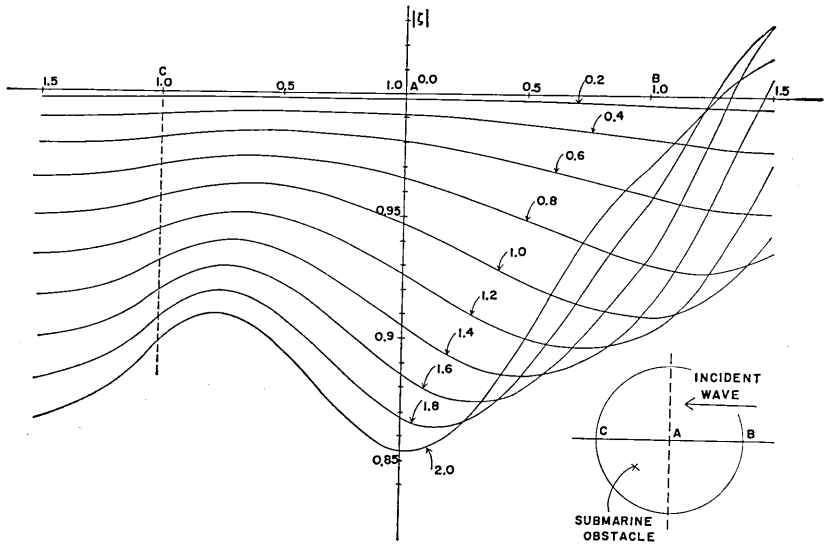

Fig. 3-2. Variation of amplitude along the x-axis for a specified ratio of depth $H_2/H_1=4/5$ (the numbers stated in the curves denote the values of kr_0).

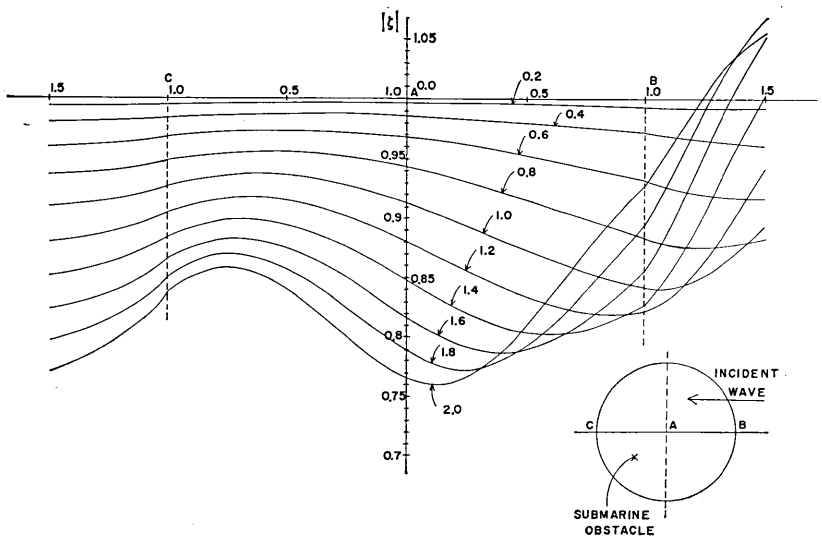

Fig. 3-3. Variation of amplitude along the x-axis for the ratio of depth $H_2/H_1=4/6$ (the numbers stated in the curves denote the values of kr_0).

(3,2) *Numerical Computations and Determination of Mesh Size*

In this section, the results of the calculations are discussed.

The calculations are carried out for the amplitude and phase in the range $kr_0=0.2$ to 2.0 along the x- and y-axis for specified values $H_2/H_1=4/5$, 4/6 and 4/7. The calculated results are visualized in Figs. 3-2, 3-3, ... and 3-13.

In Figs. 3-2, 3-3 and 3-4 showing the variations of the amplitude along the x-axis, a marked feature is found such that the waves over the obstacle, despite a concave configuration of the bottom, are not always small in height as compared with the wave heights in the outer margin of the obstacle. In the range up to $kr_0=$about 1.0, such greatness of the wave heights over the obstacle is conspicuous. Beyond this value of kr_0, the wave heights begin to grow large at the rear of the obstacle. A possible explanation of these behaviors is of a strong reflection of the waves at the forward margin of the step of the concave obstacle (C—point in Figs. 3-2, 3-3 and 3-4) in which reflected waves are likely to be powerful as compared with those at the backward margin (B—point in Figs. 3-2, 3-3 and 3-4). Through the above three figures, when kr_0 is

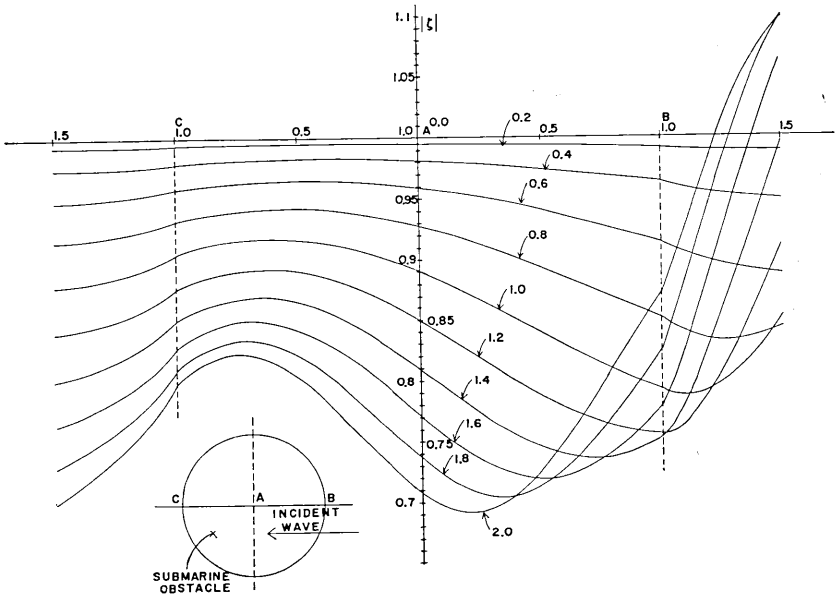

Fig. 3-4. Variation of the amplitude along the x-axis for a specified ratio of depth $H_2/H_1=4/7$ (the numbers stated in the curves denote the values of kr_0).

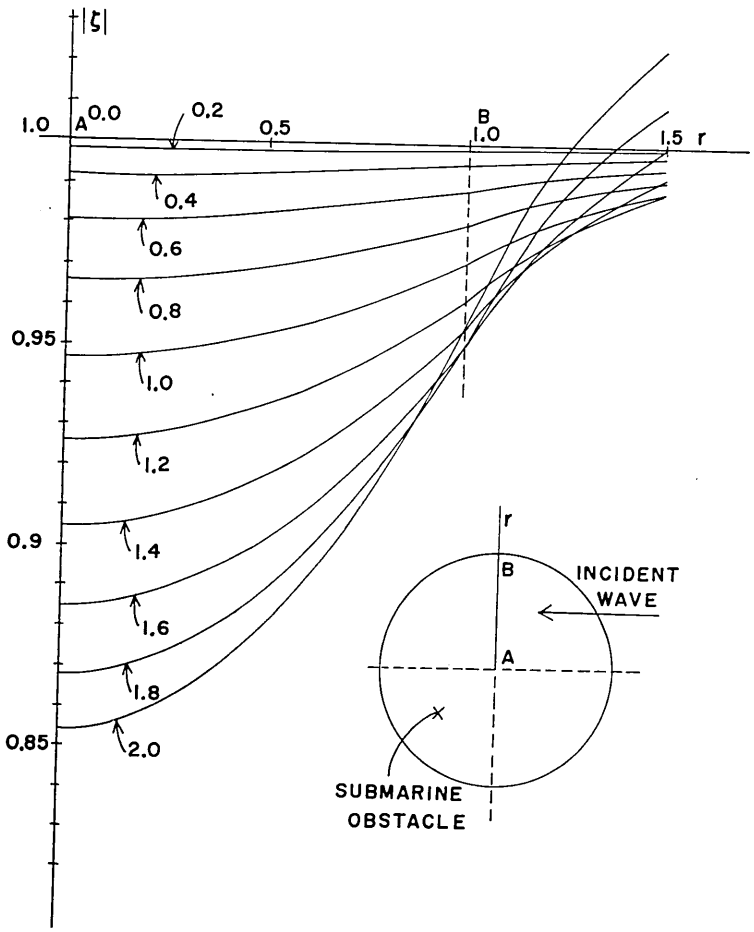

Fig. 3-5. Variation of amplitude along the y-axis for a specified ratio of depth $H_2/H_1=4/5$ (the numbers stated in the curves denote the values of kr_0).

augmented for a given H_2/H_1 or H_2/H_1 decreases for a given kr_0, the amplitude is, as a mean, decreased over the concave terrain. At a far-away point from the obstacle the amplitude, of course, tends to a unit.

Concerning the variations of the amplitude along the y-axis (refer to Figs. 3-5, 3-6 and 3-7), the amplitude diminishes toward the central part of the concave terrain to take a minimum at the very point of the center, which is the result of the diverging effect of the concave bottom. Such divergence begins to be great as H_2/H_1 begins to be small or kr_0 large.

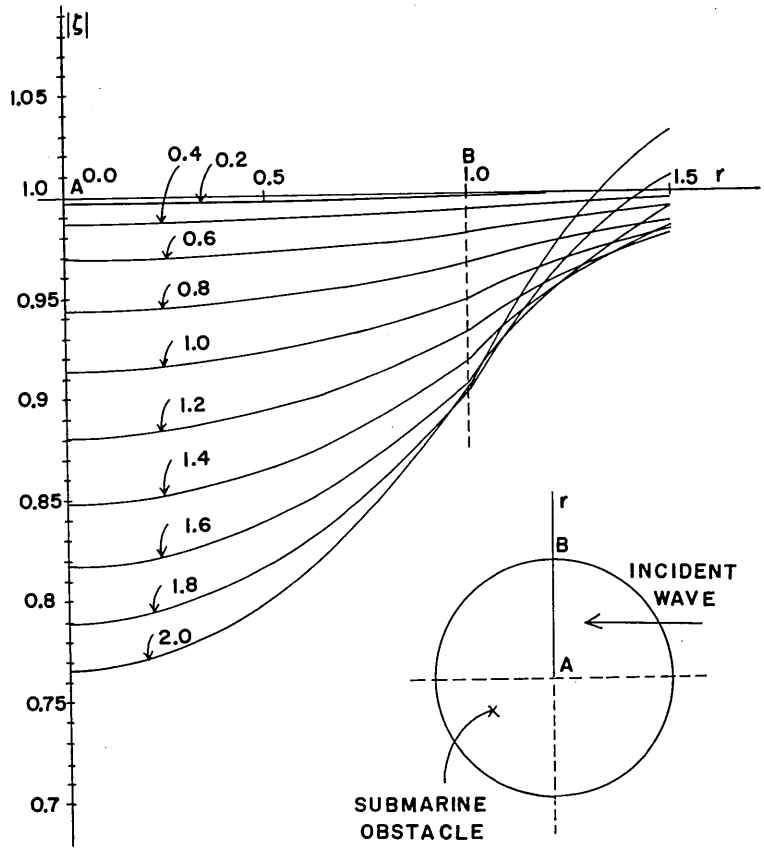

Fig. 3-6. Variation of amplitude along the y-axis for a specified ratio of depth $H_2/H_1=4/6$ (the numbers stated in the curves denote a parameter kr_0).

Let us next consider the phase variation which is shown in Figs. 3-8 to 3-13. In the first, the variation along the x-axis is noted. According to Figs. 3-8, 3-9 and 3-10, the phase at the center of the concave terrain is accelerated with an increase of kr_0 for a given H_2/H_1 or decrease of H_2/H_1 for a given kr_0. Concerning the variation along the y-axis (Figs. 3-11, 3-12 and 3-13), the component of the waves in this direction is in a sense being propagated outwards, this being caused by the divergence of the waves due to the concave submarine obstacle. Such a feature is great when kr_0 is large or H_2/H_1 small.

In the next, the determination of a mesh size is tried. For this purpose, two criterions are taken in such a way that, when a minimum

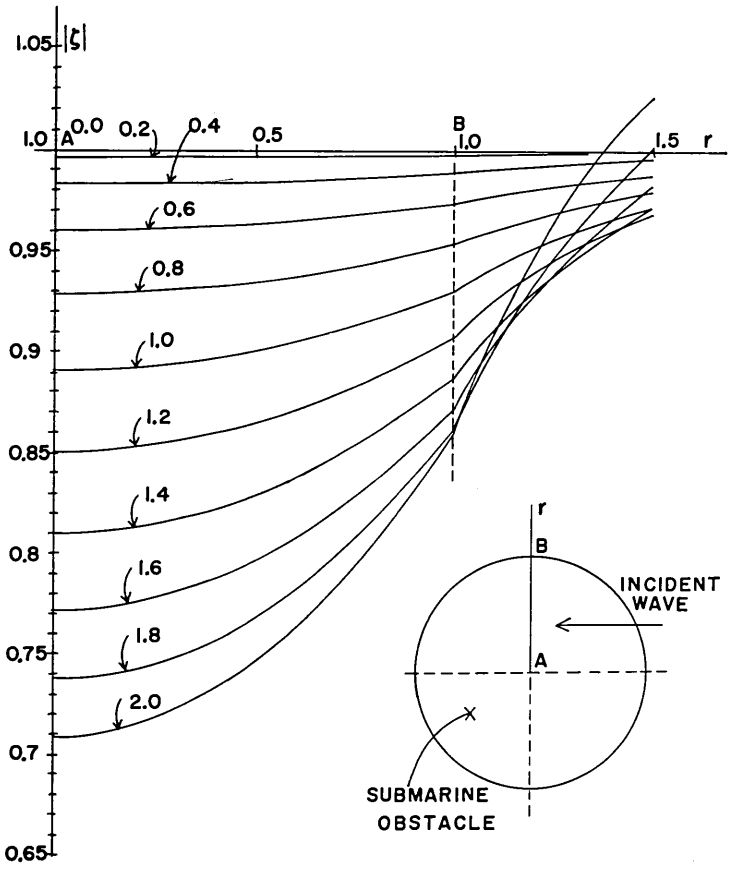

Fig. 3-7. Variation of amplitude along the y-axis for a specified ratio of depth $H_2/H_1=4/7$ (the stated numbers denote the curves relevant to a parameter kr_0).

of the amplitude near the obstacle deviates from 1.0 (the amplitude of the invading waves) by 0.1 (first criterion) and 0.05 (second one), the bottom irregularities are interpreted as being negligible.

If the first criterion is employed, the following ranges of the bottom irregularities are, from Figs. 3-2, 3-3 and 3-4, found to be neglected, i.e.,

$$kr_0=0\sim1.1 \quad \text{for } H_2/H_1=4/5\,,$$
$$kr_0=0\sim0.7 \quad \text{for } H_2/H_1=4/6\,,$$

and

$$kr_0=0\sim0.5 \quad \text{for } H_2/H_1=4/7\,,$$

A conversion of the above values to the relation of D $(=2r_0)$ to λ gives:

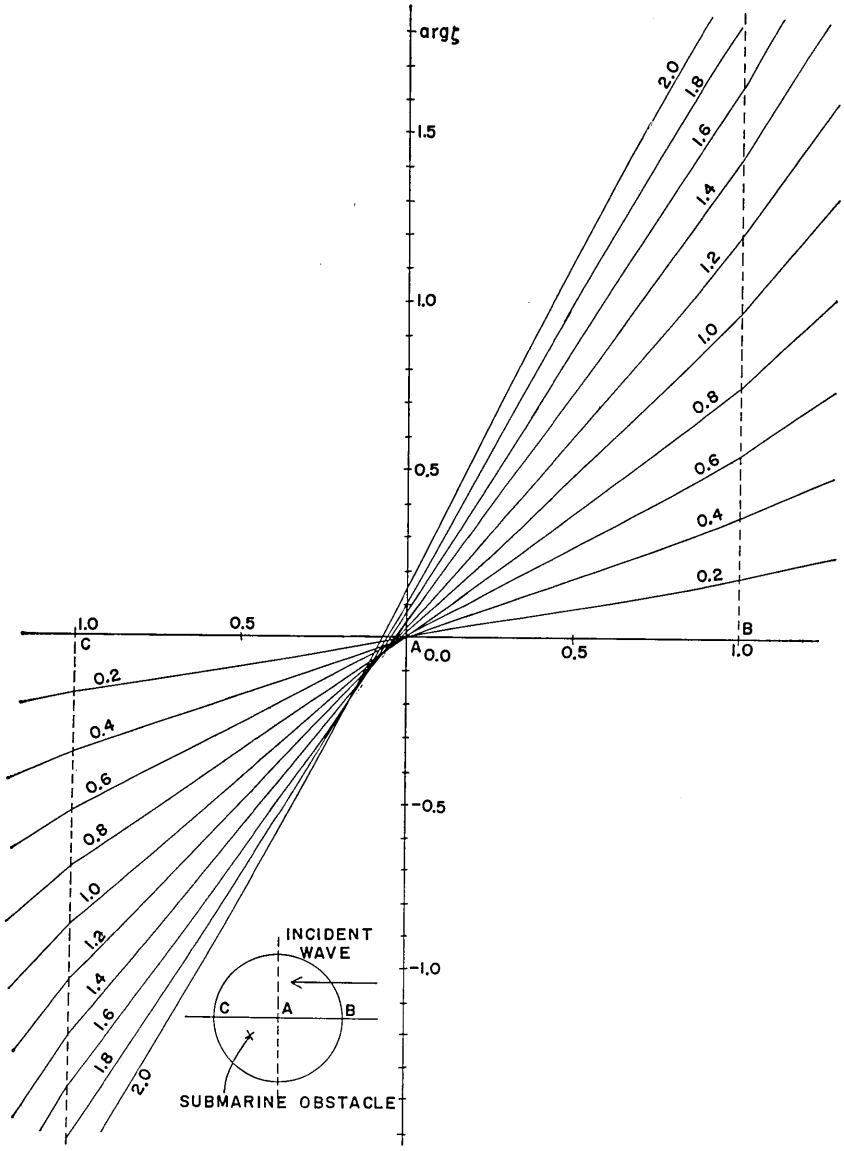

Fig. 3-8. Variation of phase along the x-axis for the ratio of depth $H_2/H_1=4/5$ (the stated numbers in the curves denote the values of kr_0).

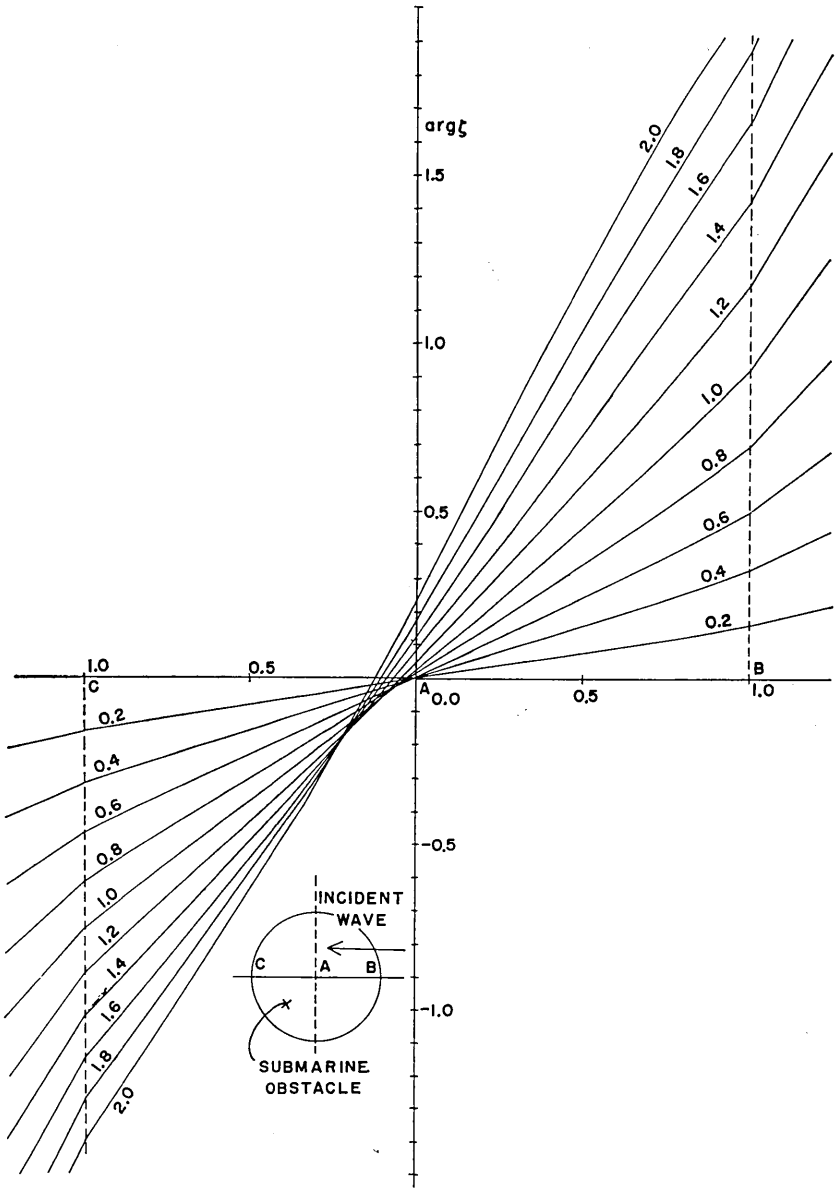

Fig. 3-9. Variation of phase along the x-axis for a specified ratio of depth $H_2/H_1=4/6$ (the stated numbers in the curves denote the values of kr_0).

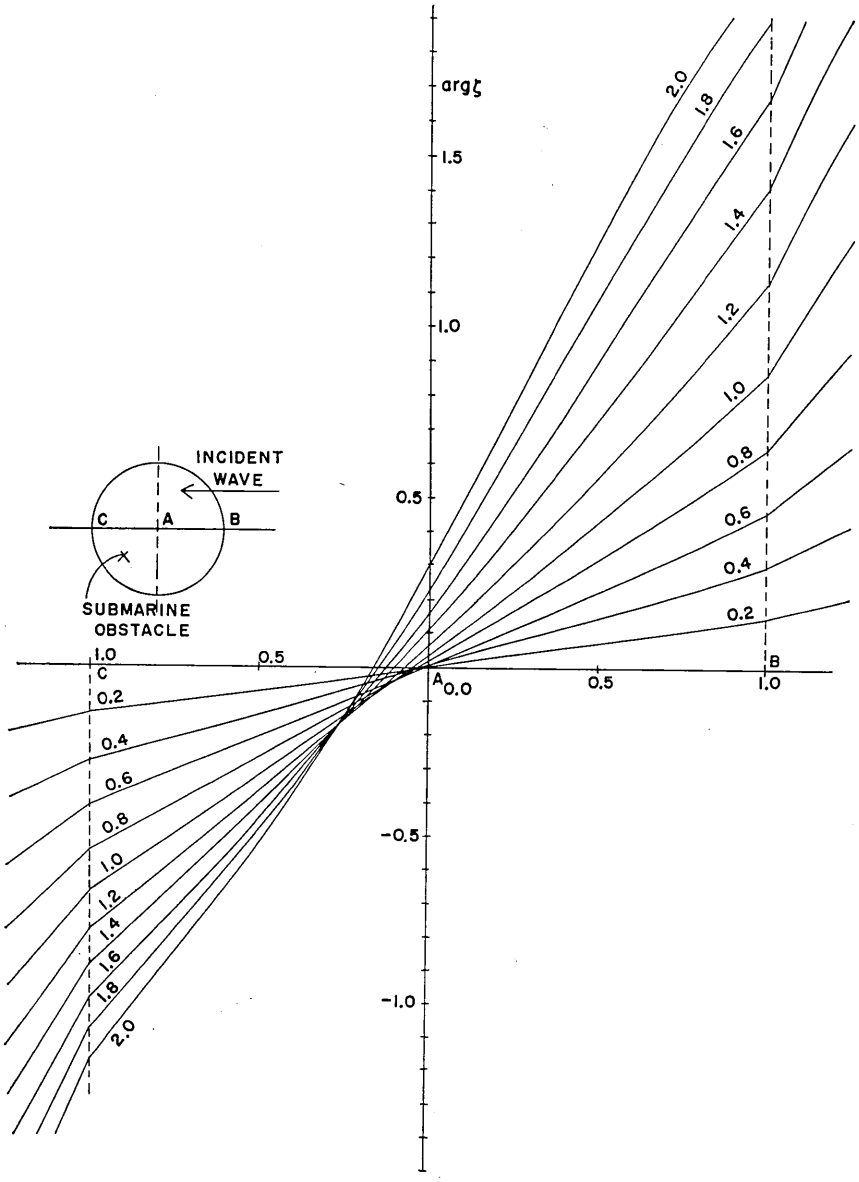

Fig. 3-10. Variation of phase along the x-axis for the ratio of depth $H_2/H_1=4/7$ (the stated numbers denote the curves relavant to a parameter kr_0).

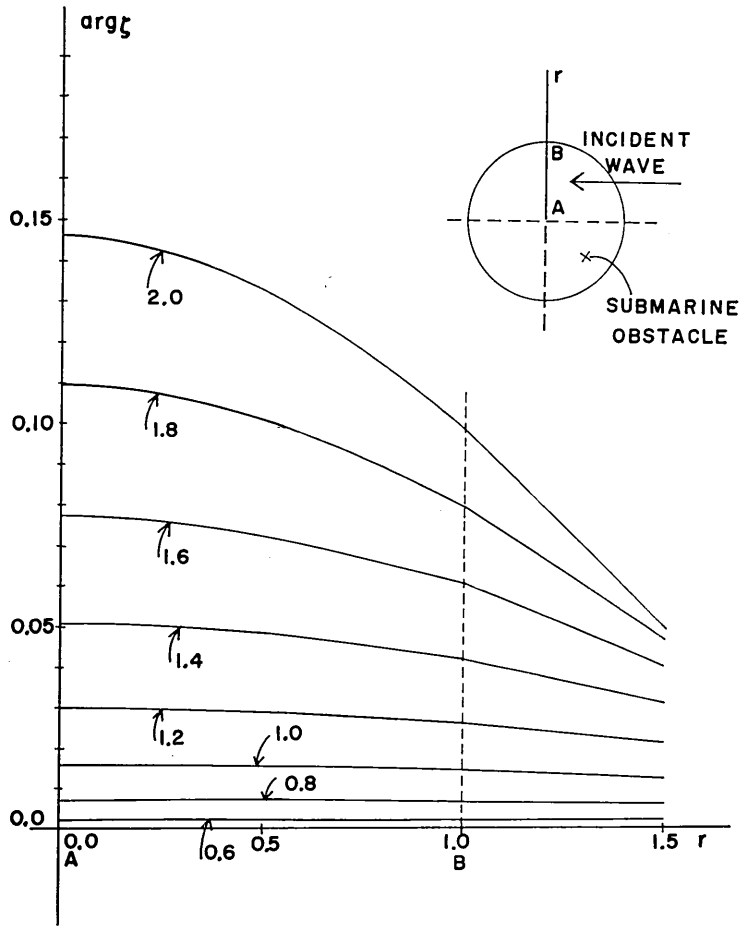

Fig. 3-11. Variation of phase along the y-axis for the ratio of depth $H_2/H_1=4/5$ (the stated numbers denote the values of kr_0).

$$\left.\begin{aligned} D/\lambda &= 0\sim 0.35 \quad \text{for } H_2/H_1=4/5\,, \\ D/\lambda &= 0\sim 0.22 \quad \text{for } H_2/H_1=4/6\,, \\ D/\lambda &= 0\sim 0.16 \quad \text{for } H_2/H_1=4/7\,, \end{aligned}\right\} \tag{3,1}$$

Taking the same examples as in Section (2,2), i.e., the Chile Tsunami and Niigata Tsunami, the estimations of the negligible scales are made as follows. Substituting the values (2,14) into (3,1), we have:—

$$\left.\begin{aligned} D &= 0\sim 168\ \text{km} \quad \text{for } H_2/H_1=4/5\,, \\ D &= 0\sim 106\ \text{km} \quad \text{for } H_2/H_1=4/6\,, \\ D &= 0\sim\ 77\ \text{km} \quad \text{for } H_2/H\ =4/7\,, \end{aligned}\right\} \tag{3,2}$$

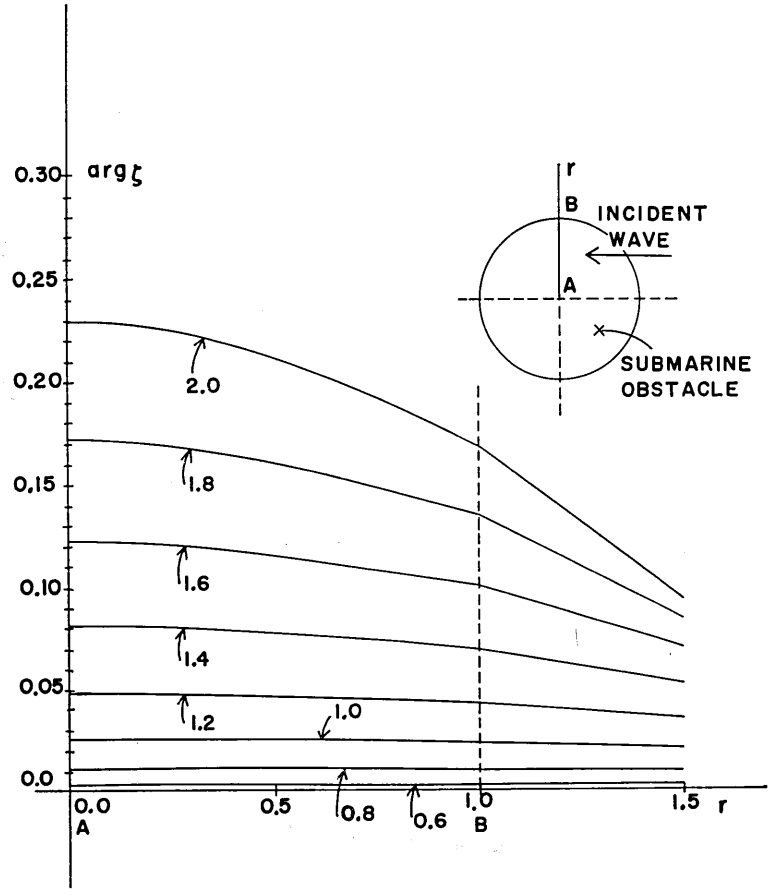

Fig. 3-12. Variation of phase along the y-axis for the ratio of depth $H_2/H_1=4/6$ (the stated numbers denote the values of kr_0).

in the case of the Chile Tsunami;

$$\left.\begin{aligned} &D=0\sim28\text{ km} \quad \text{for } H_2/H_1=4/5\,,\\ &D=0\sim18\text{ km} \quad \text{for } H_2/H_1=4/6\,,\\ &D=0\sim13\text{ km} \quad \text{for } H_2/H_1=4/7\,, \end{aligned}\right\} \tag{3,3}$$

in the case of the Niigata Tsunami.

If the second criterion is used, the ranges

$$\left.\begin{aligned} &kr_0=0\sim0.6 \quad \text{for } H_2/H_1=4/5\,,\\ &kr_0=0\sim0.4 \quad \text{for } H_2/H_1=4/6\,,\\ &kr_0=0\sim0.3 \quad \text{for } H_2/H_1=4/7\,, \end{aligned}\right\}$$

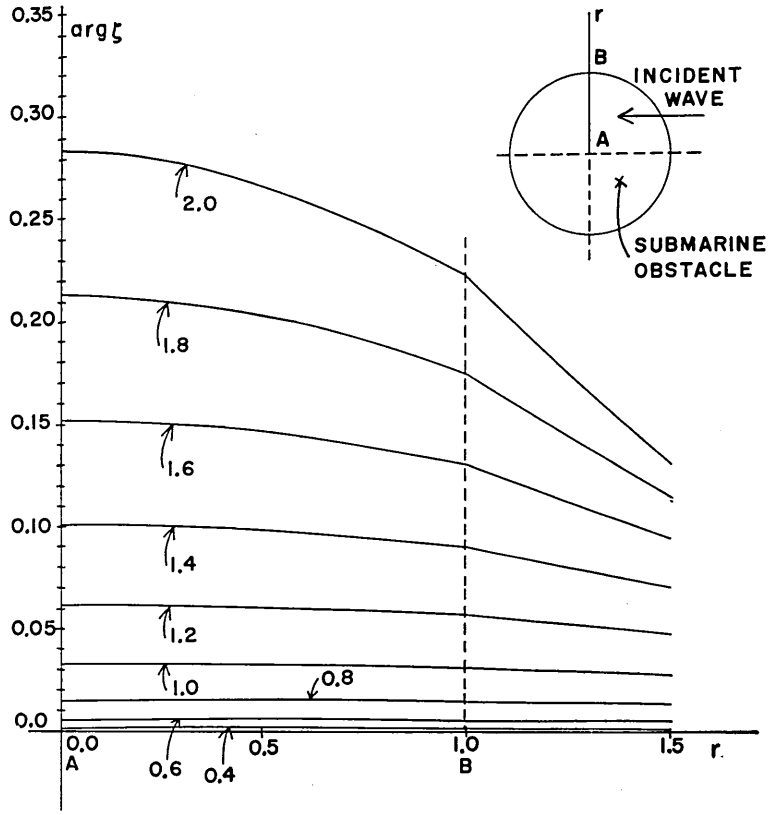

Fig. 3-13. Variation of phase along the y-axis for the ratio of depth $H_2/H_1=4/7$ (the stated numbers denote the values of kr_0).

are negligible scales of the bottom irregularities, which have been ascertained from Figs. 3-2, 3-3 and 3-4.

In a manner similar to the foregoing one, the above relations are reduced to:

$$\left.\begin{aligned} D/\lambda &= 0\sim 0.19 \quad \text{for } H_2/H_1=4/5\,, \\ D/\lambda &= 0\sim 0.13 \quad \text{for } H_2/H_1=4/6\,, \\ D/\lambda &= 0\sim 0.10 \quad \text{for } H_2/H_1=4/7\,. \end{aligned}\right\} \tag{3,4}$$

Using the wave-length of two typical tsunamis (2,14), the negligible dimensions D, under the criterion that a 5 percent deviation of the wave amplitude from that ($=1.0$) of invading waves should be neglected, become as follows from (3,4).

In the case of the Chile Tsunami,

$$\left.\begin{aligned} D&=0\sim 91\text{ km} \quad \text{for } H_2/H_1=4/5\,,\\ D&=0\sim 62\text{ km} \quad \text{for } H_2/H_1=4/6\,,\\ D&=0\sim 48\text{ km} \quad \text{for } H_2/H_1=4/7\,. \end{aligned}\right\} \tag{3,5}$$

In the case of the Niigata Tsunami,

$$\left.\begin{aligned} D&=0\sim 15\text{ km} \quad \text{for } H_2/H_1=4/5\,,\\ D&=0\sim 10\text{ km} \quad \text{for } H_2/H_1=4/6\,,\\ D&=0\sim\ 8\text{ km} \quad \text{for } H_2/H_1=4/7\,. \end{aligned}\right\} \tag{3,6}$$

In our models used in the evaluations of the negligible dimensions, the sea depth bas been kept constant, i.e. $H_2=4$, while the depth of the irregular configuration of the boutom, H_1, has been varied from 1 to 3 for the convex case and from 5 to 7 for the concave case every $\Delta H(=|H_2-H_1|)=1$. Further, the ratio of H_2 to H_1 is taken as a parameter for the calculations of the amplitude and phase. Therefore, $H_2/H_1=$ 4/1, 4/2 and 4/3 in the case of the convex bottom may be referred to $H_2/H_1=4/5$, 4/6 and 4/7 in the case of the concave one in comparing the behaviors of the waves. Comparing the dimensions to be neglected (2,13) in the case of the convex bottom and those (3,1) in the case of the concave one for the corresponding parameter H_2/H_1, it is found that the negligible dimensions for the former are, in general, smaller than those for the latter.

4. Brief Note on Scattered Waves

In this section, a brief discussion of scattered waves is presented. Let the formal expression (2,7) and (2,8) be rewritten as follows.

$$\left.\begin{aligned} \zeta_1&=\zeta_0 e^{+ikx}+\zeta_1^{(sc)}\,,\\ \zeta_2&=\zeta_0 e^{+ikx}+\zeta_2^{(sc)}\,, \end{aligned}\right\} \tag{4,1}$$

and

$$\left.\begin{aligned} \zeta_1^{(sc)}&=\sum_{m=0}^{\infty} A_m^{(1)}\cos m\theta\cdot J_m(k_1 r)-\zeta_0 e^{+ikx}\,,\\ \zeta_2^{(sc)}&=\sum_{m=0}^{\infty} A_m^{(2)}\cos m\theta\cdot H_m^{(2)}(k_2 r)\,. \end{aligned}\right\} \tag{4,2}$$

Then $\zeta_1^{(sc)}$ and $\zeta_2^{(sc)}$ in (4,2) imply the scattered waves produced by the

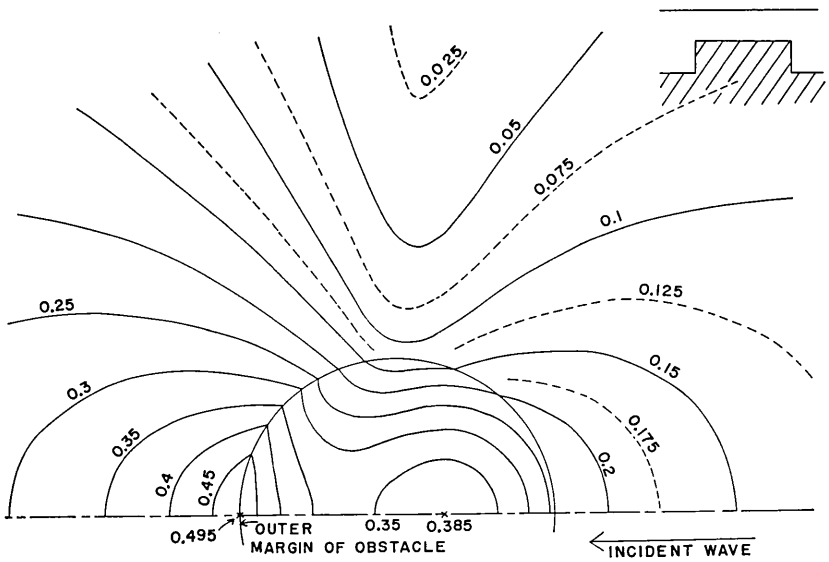

Fig. 4-1. Amplitude variation of the scattered waves $\zeta^{(sc)}$ around a convex bottom for a specified parameter $kr_0=1.0$ (the stated values in the figure denote $|\zeta^{(sc)}|$, the inserted figure on the right-hand side of the above figure being a profile of a used model).

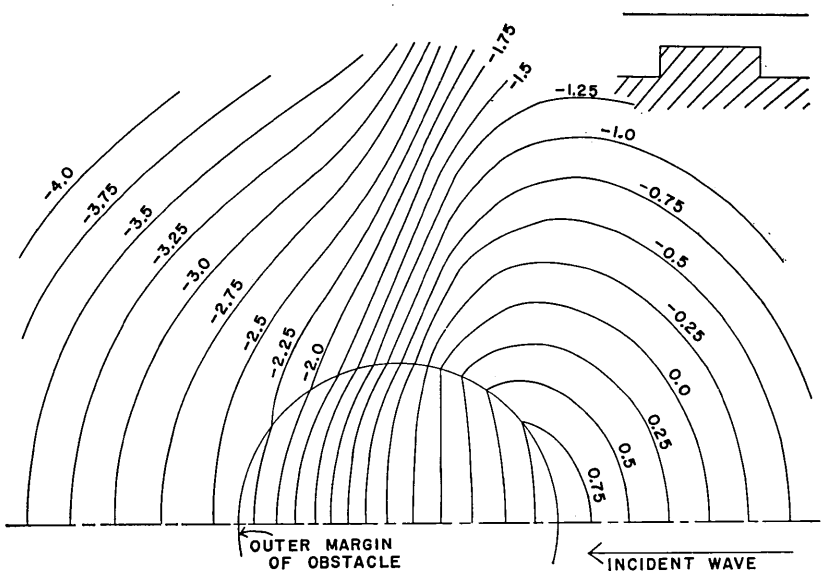

Fig. 4-2. Phase variation of the scattered waves $\zeta^{(sc)}$ around a convex bottom for a specified parameter $kr_0=1.0$ (the stated values in the figure denote $\arg \zeta^{(sc)}$, the inserted figure on the right-hand side of the above figure being a profile of a used model).

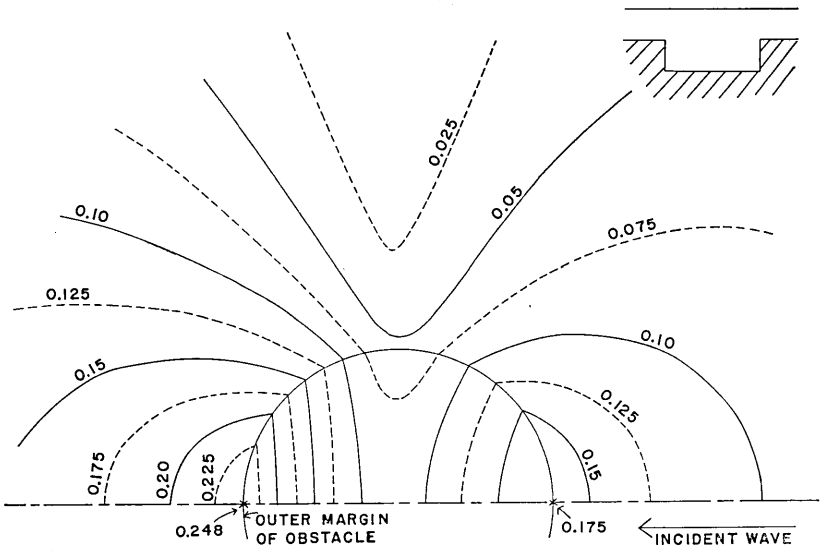

Fig. 4-3. Amplitude variation of the scattered waves $\zeta^{(sc)}$ around a concave bottom for a specified parameter $kr_0=1.0$ (the stated values in the figure denote $|\zeta^{(sc)}|$, the small figure in the above figure being a profile of a used model.)

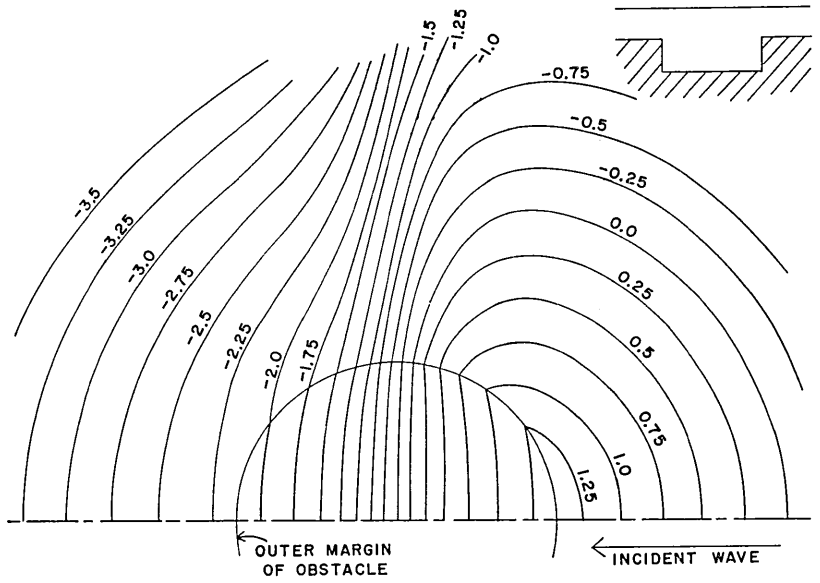

Fig. 4-4. Phase variation of the scattered waves $\zeta^{(sc)}$ around a concave bottom for a specified parameter $kr_0=1.0$ (the stated numbers in the figure denote $\arg \zeta^{(sc)}$, the small figure being a profile of a used model).

irregularities of the bottom. When the bottom is horizontal without any obstacle, the formal expressions ζ_1 and ζ_2 are reduced to a form

$$\zeta_0 e^{+ikx}$$

as a result of disappearance of the terms $\zeta_1^{(sc)}$ and $\zeta_2^{(sc)}$.

Using (4,2), the overall variations of the amplitude and phase of the scattered waves are sketched in Figs. 4-1 to 4-4 for a few specified values of H_2/H_1 and kr_0

According to Figs. 4-1 and 4-2 showing the amplitude and phase for $H_2/H_1=4/2$ and $kr_0=1.0$ (the case of a convex bottom), it is found that (1) a small mount of the amplitude implying the convergence of the waves appears above the submarine obstacle (Fig. 4-1), (2) the scattered waves are directed mainly along the line of the incidence of the waves, which are seen from both figures of the amplitude and phase (Figs. 4-1 and 4-2), and (3) the scattered waves are emitted from the backward margin of the obstacle (the side of the incidence of the waves) (Figs. 4-2).

For the scattered waves in the case of a concave bottom ($H_2/H_1=4/6$ and $kr_0=1.0$), similar behaviors are found. That is to say, referring to Figs. 4-3 and 4-4, the former of which denotes the variation of the amplitude and the latter that of the phase, (1) the waves are scattered primarily in the direction of the incidence of the waves (Figs. 4-3 and 4-4), and (2) the scattered waves are ejected from the backward margin of the circular obstacle. Such resemblance of the behaviors of the scattered waves in the cases of convex and concave bottoms is rather surprising. The only difference in the two cases is that the scattered waves above the submarine obstacle for the case of a concave bottom have a relatively small amplitude in the middle part of the obstacle, above all, near the outer margin in the direction perpendicular to the axis of the incidence of the waves, while the amplitude of the scattered waves for the case of a convex bottom makes up a small mount near the midpoint of the obstacle. The above low amplitude for the case of a concave bottom is caused by a total reflection at the outer margin of the obstacle in addition to the diverging effect of the bottom.

71. 凸または凹型の海底のまわりの長波

地震研究所　桃　井　高　夫

本報告において，凸または凹型の海底のまわりの長波が論じられ，電子計算機による津波屈折図作製の際の有効網目の長さ (effective mesh length) の決定がおこなわれている．とくに，海底凹凸にもとづく散乱波の状態について，二三論及されている．